Lasers in Manufacturing Conference 2017

# Nanosecond laser ablation of different crystallographic planes of sapphire

Fatemeh Saeidi[a], Freidy Mouhamad Ali[b], Kilian Wasmer[a,*]

[a]*Laboratory for Advanced Materials Processing (LAMP), Swiss Federal Laboratories for Materials Science and Technology (Empa), Feuerwerkerstrasse 39, 3602 Thun, Switzerland*
[b]*Rollomatic SA, Rue des Prés Bugnons 3, 2525 Le Landeron, Switzerland*

**Abstract**

In this work, nanosecond laser ablation of different crystallographic planes (c-, a- and m-plane) of sapphire produced by Verneuil, Kyropoulos, and EFG methods have been studied. The ablation thresholds as well as the crack orientations were analyzed by single laser shots at different laser fluence ranging from 4 to 200 J/cm$^2$. The results showed that the production methods and the orientation planes of sapphire have slight effect on both the ablation threshold and the ablated depth of sapphire. However, the crack morphology strongly depends on the planes orientations.

Keywords: Sapphire; ns-laser ablation; crystallographic plane

## 1. Introduction

Sapphire, the single crystal form of $Al_2O_3$, presents numerous promising optical, thermal, and mechanical properties. Its refractory ($T_m$= 2046°C (Weber, 2002)) and insulating behaviors (band gap ~ 9.9 eV (Weber, 2002)) as well as its transparency over a wide range of wavelength (0.2-5 µm (Dobrovinskaya, Lytvynov, and Pishchik, 2009) make sapphire a desired candidate for windows glasses and optical lenses exposed to harsh environments (Zhao, Huang, and Kang, 2012). The high hardness (9 Mohs (Dobrovinskaya et al., 2009)) and high wear resistance in conjunction with the chemical stability and inertness of sapphire have broadened the application of this material to many engineering and medical instruments (Dobrovinskaya et al., 2009).

* Corresponding author. Tel.: +41-58-765-6271; fax: +41-58-765-6990.
*E-mail address:* kilian.wasmer@empa.ch.

The precise cutting and machining of sapphire are still challenging due to its high hardness and brittleness. Laser machining is an interesting alternative to the conventional methods (e.g. diamond drilling and grinding), which allows 3D microfabrication of hard materials without the need of expensive machining tools. However, the fundamentals of laser-sapphire interaction are not fully understood and still needs to be further investigated. It has been reported that different crystallographic planes of sapphire has different thermal and optical properties (Belyaev, 1980; Dobrovinskaya et al., 2009). The mechanical properties of sapphire also depend on both the crystallographic orientation and its manufacturing technique (Graça et al., 2014). Several techniques such as Verneuil, Kyropoulos, EFG (Edge-Defined Film-Fed Growth), and Czochralski exist for the sapphire production, and the presence of defects in the crystal of sapphire is shown to be correlated to its production method (Graça et al., 2014). The effect of the different crystal orientations in sapphire has been studied before for fs-laser but, as it is known, the ablation mechanism is different in ns- and fs-lasers. Therefore, it is of high interest to determine the effect of crystal orientations for a ns-laser. In addition, there is no study on the effect of sapphire production method on its laser ablation behavior. In this work, nanosecond laser ablation of different crystallographic planes (*c*-, *a*- and *m*-plane) of sapphire produced by Verneuil, Kyropoulos, and EFG methods was studied.

## 2. Experiments

Single crystal sapphire samples with different crystal orientations (*c*-, *a*-, *m*-plane) produced by the Kyropoulos, Verneuil, and EFG techniques were used in this study. Only *a*-plane of the sapphire sample produced by EFG method was considered in this study. The plane orientations of the studied samples are shown schematically in Fig. 1. Each plane has a maximum misorientation angle of 2°. All the samples were polished and their surface roughness was $R_a$ = 23 ± 7 nm.

The laser machining tests were carried out using a ns-laser with a wavelength in the visible range and an

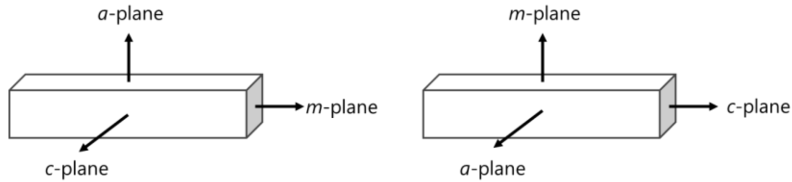


Fig. 1. The plane orientations of the sapphire samples, which were produced by Verneuil, Kyropoulos, and EFG method. Only *a*-plane of a sapphire sample produced by EFG method was ablated in this study.

average output power of 16 W. The single shot ablation threshold was calculated for the different crystallographic planes of sapphire based on the variation of the ablated spot's diameter for single shots at different pulse energies ($E_P$) or the so-called $D^2$-method (Liu, 1982). According to this method, the squared diameter of an ablated area is correlated to $E_P$ by:

$$D^2 = 2w_0^2 \, ln\left(\frac{E_P}{E_{th}}\right) \tag{1}$$

where $D$ is the diameter of an ablated area at a specific energy ($E_P$), $w_0$ is the beam radius at the $1/e^2$ intensity, and $E_{th}$ is the energy per pulse at the ablation threshold. $w_0$ can be calculated from the slope of the

linear plot of the measured squared diameter of the craters ($D^2$) as a function of the logarithm of $E_P$. The peak ablation threshold fluence for a Gaussian beam can then be calculated by:

$$\text{Peak } F_{th} = \frac{2E_P}{\pi w_0^2} \quad (2)$$

and the average ablation threshold can simply be calculated by $E_P/\pi w_0^2$.

The ablated areas were observed and their diameters were defined using an optical microscope and a field emission scanning electron microscope (Hitachi S-4800, Japan). For the threshold calculations, the diameter of four craters was measured for each set of laser parameters. The depth and the profile of the ablated area were defined by a confocal microscope (Keyence VK-X260K, Japan). Using a power meter (Gentec-EO, Canada), the average output energy of the laser was precisely measured for each set of parameters to calculate the $E_p$.

## 3. Results and discussion

### 3.1. Ablation threshold fluence

Fig. 2 shows the variation of the measured squared diameter of the craters ($D^2$) as a function of the applied pulse energy for the *a*-plane of a sapphire sample produced by the Kyropoulos method. As mentioned in Section 2, the slope of the logarithmic fit of this plot determines the beam radius at the 1/e$^2$ intensity. For this sample, $w_0$ is calculated to be 22 µm, and the corresponding peak ablation threshold fluence was 28.5 J/cm$^2$. The calculated ablation thresholds for all other samples are determined with the same method and are summarized in Table 1. As seen in this table, for the sapphire samples produced by Kyropoulos and Verneuil methods, the threshold fluence of *a*-plane is higher than *c*- and *m*-planes, while *c*- and *m*-planes have comparable threshold ($F_{\text{th, }a\text{-plane}} > F_{\text{th, }c\text{-plane}} \approx F_{\text{th, }m\text{-plane}}$). The *a*-plane of the sapphire sample produced by Verneuil method has lower value compared to the samples produced by Kyropoulos and EFG. This might be related to the higher mosaicity in *a*-plane of sapphire produced by Verneuil method, which could enhance its absorption.

### 3.2. Ablated depth

The variations of the ablated depth as a function of the applied average fluence ($F_{ave}$) for the *a*-, *c*-, and *m*-planes of sapphire samples produced by the Kyropoulos and Verneuil methods are illustrated in Fig. 3. As evident from this figure, there is no distinct difference in the ablated depth of different crystallographic planes of the samples produced with the Verneuil method. However, the Kyropoulos sample shows small difference in depth. The *m*-plane of this sample has slightly higher depth compared to *a*- and *c*-plane. For the Kyropoulos sample, a higher scatter is also observed between the depths of different shots ablated with the same average fluence. This can be explained by the fact that the number of defects in Kyropoulos sample is lower than the samples produced by the Verneuil method. As defects highly affect the absorption of laser in such transparent materials, for a sample with lower density of defects, the probability of absorption is lower

Table 1. Ablation threshold for different planes of Sapphire produced by Kyropoulos, Verneuil, and EFG methods.

| Production method | **Kyropoulos** | | | **Verneuil** | | | **EFG** |
|---|---|---|---|---|---|---|---|
| Crystallographic planes | *a*-plane | *c*-plane | *m*-plane | *a*-plane | *c*-plane | *m*-plane | *a*-plane |
| Peak $F_{th}$ [J/cm$^2$] | 28.5 | 23.4 | 23.9 | 26.9 | 25.4 | 25.7 | 28.3 |
| Average $F_{th}$ [J/cm$^2$] | 14.2 | 11.7 | 12.0 | 13.5 | 12.7 | 12.9 | 14.2 |

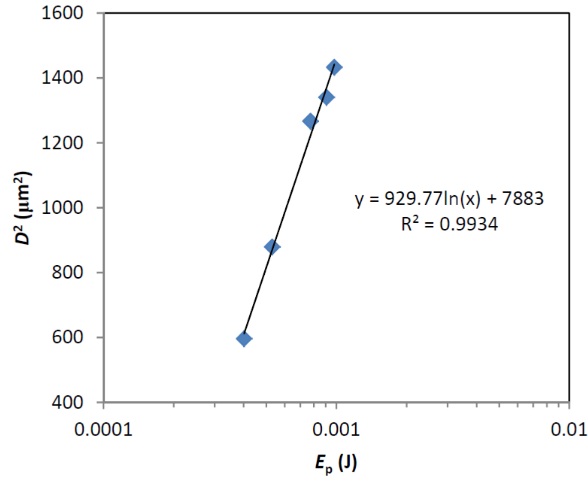


Fig. 2. Squared diameter of the ablated area ($D^2$) as a function of the applied pulse energy ($E_P$) for the a-plane of a single crystal sapphire produced by the Kyropoulos method.

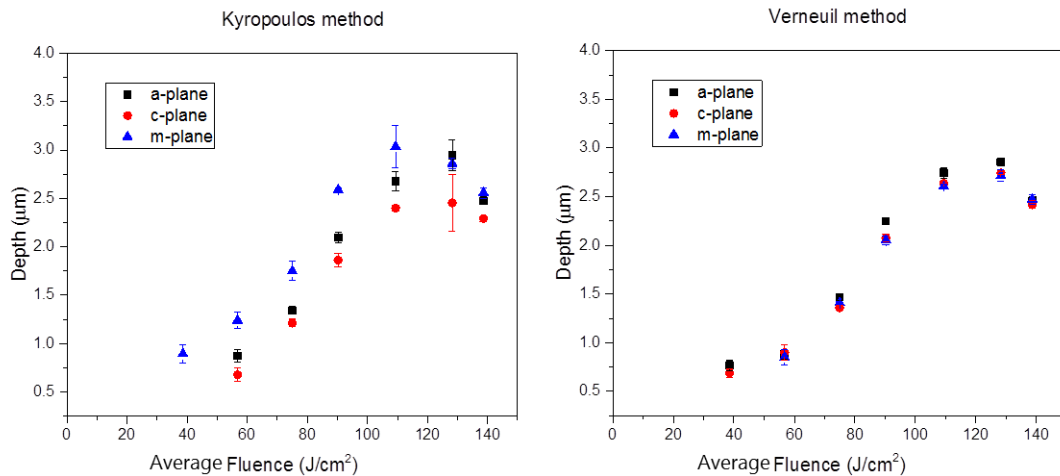


Fig. 3. Ablated depths as a function of the average fluence ($F_{ave}$) for the different planes of sapphire, which are produced by the Kyropoulos and Verneuil methods.

and not the same for different parts of the surface.

In Fig. 4, the variations of the ablated depth versus the average fluence for the *a*-plane of sapphire are compared for the different methods of production. As seen in this figure, the ablated depth in *EFG* sample is slightly higher than the Kyropoulos and Verneuil samples for the average fluence between 75 and 109 J/cm$^2$. In general, from the results obtained for the fluence threshold and the ablated depth, it can be concluded that the different crystallographic planes and also the production method of sapphire have negligible effect on the ablation of sapphire.

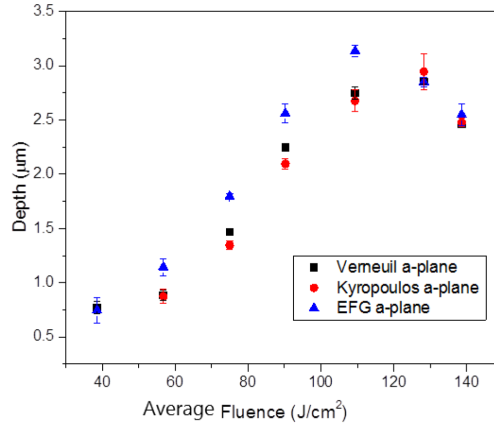


Fig. 4. Ablated depths as a function of the average fluence ($F_{ave}$) for the *a*-plane of sapphire samples produced by the Kyropoulos, Verneuil and EFG methods.

### *3.3. Cracks morphology*

The cracks morphology of single shots produced on different crystallographic planes of the Kyropoulos and Verneuil samples were characterized using optical and scanning electron microscopies. Fig. 5 displays the optical images of the cracks formed on the different planes of the Kyropoulos sample. The average fluence, at which the cracks could be detected easily by optical microscopy, is written on each image. As evident from this figure, the morphology of cracks is different for each plane of sapphire.

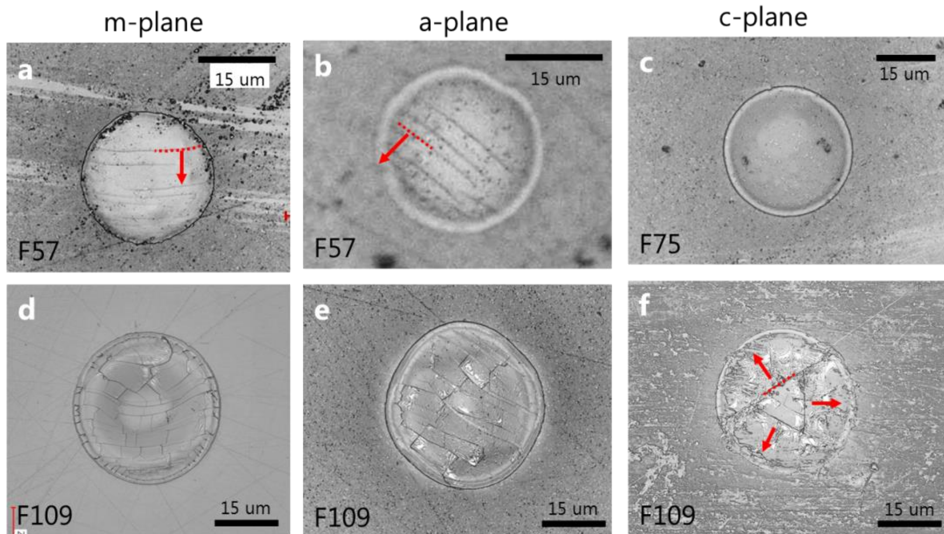


Fig. 5. Cracks orientation forms on the different crystallographic planes of sapphire produced by the Kyropoulos method.

On both *a*- and *m*-planes, parallel cracks were always visible on the ablated spot, even at a very low fluence ($F_{ave} \approx 21$ J/cm$^2$). Fig. 5a and b illustrate the parallel cracks morphology formed on these planes at an average fluence of 57 J/cm$^2$. For the lower fluence ($F_{ave} < 57$ J/cm$^2$), cracks were detectable on both Verneuil and Kyropoulos samples with the help of an SEM. However, as expected, the Verneuil samples showed lower crack resistivity. As seen in Fig. 5d and e, in these planes, by increasing the $F_{ave}$, cracks connect to each other with a random orientation.

On the contrary, the *c*-plane of sapphire does not show any cracks at low average fluence ($F_{ave} < 90$ J/cm$^2$). At higher fluence, cracks are seen in three main axes (see Fig. 5f).

Considering the lattice structure of the sapphire including its crystallographic planes, it can be concluded that the parallel cracks, which were observed on the *a*-plane, form in $<10\bar{1}1>$ direction. Cracks on the *m*-planes are in the direction of $<11\bar{2}0>$. The *c*-plane of sapphire seems to be the strongest to crack, as no parallel cracks are seen at low fluence ($F_{ave} \leq 90$ J/cm$^2$). This can be explained by the higher strength and crack resistance of this plane (Dobrovinskaya et al., 2009). By further increasing the fluence, cracks created on this plane forms a rectangle (see Fig. 5f). The crack direction of these cracks is not yet clear to the authors. However, it is known that the slip direction on this plane occurs in $<10\bar{1}0>$ and $<1\bar{2}10>$ directions (Dobrovinskaya et al., 2009). As *a*-plane $(1\bar{2}10)$ of sapphire is stronger than *m*-plane $(10\bar{1}0)$ (Graça et al., 2014), it is possible to assume that these cracks forms in the direction of *m*-plane.

## 4. Conclusion

In the present work, ns-laser ablation of single crystal sapphire samples produced with different production methods (Verneuil, Kyropoulos, and EFG) was studied. In order to characterize the effect of the plane orientations on the ablation threshold and the crack morphology, single shots with different fluence were produced on different crystallographic planes of sapphire. The results showed that, using a ns-laser, the ablation threshold as well as the ablated depth in sapphire is not that much sensitive to the production methods and the crystallographic orientation of the planes. However, the cracks morphology and cracking resistivity strongly depends on the plane orientation. In general, Kyropoulos samples displayed higher resistivity to cracks formation, and among the studied planes, *c*-plane was the strongest to crack formation.


## Acknowledgements

The authors would like to thank the Swiss Commission for Technology and Innovation (CTI – project N° 18210 PFIW-IW) and Rollomatic SA for the financial support of this work.


## References


Belyaev, L. M., 1980. Ruby and sapphire (1st ed.). New Delhi: Amerind.

Dobrovinskaya, E. R., Lytvynov, L. A., and Pishchik, V., 2009. Sapphire. Springer.

Graça, S., Trabadelo, V., Neels, A., Kuebler, J., Le Nader, V., Gamez, G., Wasmer, K., 2014. Influence of mosaicity on the fracture behavior of sapphire, Acta Materialia *67*, p. 67.

Liu, J. M., 1982. Simple technique for measurements of pulsed Gaussian-beam spot sizes, Optics Letters *7*, p. 196.

Weber, M. J., 2002. Handbook of Optical Materials. USA: CRC Press.

Zhao, M., Huang, Y., and Kang, J. U., 2012. Sapphire ball lens-based fiber probe for common-path optical coherence tomography and its applications in corneal and retinal imaging, Optics Letters *37*, p. 4835.